Theoretical and Applied Climatology (2021) 144:711–722
https://doi.org/10.1007/s00704-021-03563-7

ORIGINAL PAPER

On the cause-and-effect relations between aerosols, water vapor, and clouds over East Asia

Stavros Stathopoulos[1] · Anastasios A. Tsonis[2,3] · Konstantinos Kourtidis[1]

Received: 15 March 2020 / Accepted: 9 February 2021 / Published online: 24 February 2021

Abstract
Atmosphere is a complex dynamical system. Here, we investigated the causal links between aerosols, water vapor, and clouds, using the convergent cross mapping (CCM) method, which is based on nonlinear state space reconstruction. We utilized remote sensing data of aerosol optical depth at 550 nm (AOD), water vapor (WV), cloud cover (CC), cloud optical depth (COD), cloud effective radius-ice (CERI), and cloud effective radius-liquid (CERL) from Moderate Resolution Imaging Spectro-radiometer (MODIS) sensor over East Asia, for the period 2003–2018. Our analysis shows that there is a bidirectional forcing between AOD, CC, and COD which could be attributed to the invigoration effect of aerosols on clouds. In addition, there is a bidirectional forcing between AOD and WV and AOD and CERL, which could be attributed to the first indirect effect of aerosols on clouds, while there is no causality among AOD and CERI, probably because of strong coupling among aerosols and ice nuclei. Based on our analysis, we conclude that CCM method can effectively be used in all aerosol–cloud interactions' studies, searching for causality among the parameters.

1 Introduction

The intricate impact of aerosols on climate has drawn the attention of the scientific community for decades, stimulating efforts to disentangle their role in climate change (Koren et al. 2005; Andreae and Rosenfeld 2008; Grandey et al. 2013; Kant et al. 2019). Aerosols absorb and scatter radiation, which is denoted as "direct aerosol effect" (Haywood and Boucher 2000). In addition, aerosols can modify cloud properties by acting as cloud condensation nuclei (CCN), leading to smaller and more numerous cloud droplets, increasing cloud albedo, a process known as "first aerosol indirect effect" or "Twomey effect" (Twomey 1974; Liu and Li 2018). These cloud droplets may delay the onset of collision–coalescence mechanisms inside the cloud, inhibiting precipitation and increasing their lifetime, a process known as "second aerosol indirect effect" (Albrecht 1989; Jones and Christopher 2010). Furthermore, absorbing aerosols such as soot, dust, and black carbon, can suppress cloud formation by warming the atmosphere, resulting into the increase of water vapor evaporation, thinning the clouds, a process known as "semi-direct aerosol effect" (Hansen et al. 1997; Ackerman et al. 2000; Huang et al. 2006).

Researchers have used a lot of different approaches to investigate the aerosol–cloud interactions, either by using remote sensing and ground-based measurements (Zhang et al. 2015; Zhao et al. 2018a; Shi et al. 2019), or by utilizing climate models (Park et al. 2018; Hodzic and Duvel 2018; Kudzotsa et al. 2019), or even by coupling measurements with climate models (Eck et al. 2018; Solomos et al. 2019). Our research is based on a different approach. It utilizes remote sensing data from the Moderate Resolution Imaging Spectro-radiometer (MODIS) sensor, onboard Aqua satellite, with the convergent cross mapping (CCM) method (Sugihara et al. 2012). CCM is a data-based method that can detect causality in complex nonlinear systems with low computational cost

✉ Stavros Stathopoulos
sstathop@env.duth.gr

Anastasios A. Tsonis
aatsonis@uwm.edu

Konstantinos Kourtidis
kourtidi@env.duth.gr

1 Laboratory of Atmospheric Pollution and Pollution Control Engineering of Atmospheric Pollutants, School of Engineering, Democritus University of Thrace, 12 Vas. Sofias Str, 67100 Xanthi, Greece

2 Department of Mathematical Sciences, Atmospheric Sciences Group, University of Wisconsin-Milwaukee, Milwaukee, WI, USA

3 Hydrologic Research Center, San Diego, CA, USA

(Clark et al. 2015). It has been used successively in many different scientific areas, detecting bidirectional or synchronous forcings between historical time series of different variables (Heskamp et al. 2014; Tsonis et al. 2015; Zhang et al. 2019). Here, we employed CCM method to investigate causal relations between aerosols, water vapor, and clouds over East Asia (20°–45° N, 105°–122.5° E).

East Asia (EA) region is characterized by high level of air pollution due to its fast-economic growth and population increase in the last decades (Li et al. 2011). It is strongly affected by substantial anthropogenic emissions, which deteriorates the air quality and has a detrimental impact on population's health (Wang et al. 2014b). EA region is dominated by mineral dust, mainly transported from Taklimakan and Gobi deserts during late winter and early spring seasons (Huang et al. 2008), as well as from sea salts, transported from the nearby Pacific Ocean (Wang et al. 2014a).

The aim of this paper is to investigate causality between aerosols, water vapor, and clouds using remote sensing data over EA region, for the period July 2003–December 2018. This study is structured as follows: Section 2 provides information about the utilized data, the description of CCM method, and the methodology followed for the investigation of the causal relations between the data. The results of the analysis are presented and discussed in Section 3. Finally, our findings are summarized in Section 4.

2 Data and methods

2.1 MODIS aerosol, water vapor, and cloud products

The Moderate Resolution Imaging Spectro-radiometer (MODIS) is a passive remote sensing sensor onboard two satellites, Terra and Aqua. Aqua was launched in May 2002 at an orbit of approximately 700 km above Earth, having an overpass time at about 13.30 local time (LT). MODIS sensor has a swath of approximately 2300 km, covering the entire globe daily. It measures not only the reflected solar radiance but also the terestrial radiation in 36 spectral bands (Levy et al. 2007), providing products at different spatial and temporal resolutions. In particular, the user can choose from the Level-2 (L2) (daily products at 10-km and 3-km resolutions) and the Level-3 (L3) (daily, 8-day, monthly) products at 1° × 1° horizontal resolution. L3 are derived from the L2 products, after being spatiotemporarely aggregated (Platnick et al. 2015; Hubanks et al. 2019).

Aerosol products from MODIS are provided in three different datasets, namely the Dark Target (DT), Deep Blue (DB) and the combined Dark Target–Deep Blue (DTB) datasets. The DT and DB aerosol datasets are generated from the updated second-generation DT algorithm (Levy et al. 2013) and the enhanced DB algorithm (Hsu et al. 2013), respectively. The DTB aerosol dataset is generated from the merging of DT and DB aerosol datasets, after the application of three criterias, according to the Normalized Difference Vegetation Index (NDVI). In particular, if NDVI is greater than 0.3, the DT retrievals are used. If NDVI is between 0.2 and 0.3, then the average value of DB and DT retrievals is used. Finally, if NDVI is less than 0.2, then the DB retrievals are used (Levy et al. 2013). The water vapor and cloud products from MODIS are derived using different retrieval algorithms. The water vapor product is derived using an algorithm that calculates the atmospheric water vapor transmittances, based on theoretical radiative transfer calculations and Look-Up-Table (LUT) procedures (Gao and Kaufman 1998). The cloud cover product is derived using clear versus cloudy discrimination in a given MODIS field-of-view (FOV), after performing a numerous spectral and/or spatial variability tests and calculating clear sky confidences for each test applied, which are combined into a preliminary overall confidence of clear sky for the FOV. Then, the final output confidence is determined as one of four categories: confident clear, probability clear, probably cloud or confident cloud, in conjunction with statistics derived from collocated Cloud-Aerosol Lidar with Orthogonal Polarization (CALIOP) cloud products and MODIS radiance data (Team M C M et al. 2010). The cloud optical depth and cloud effective radius for liquid and ice clouds products are produced utilizing an optical/microphysical algorithm that uses six visible, near-infrared, shortwave-infrared, midwave-infrared, and several thermal MODIS channels, and comparing these measurements with theoretical forward model calculations as in Nakajima and King (1990) (Platnick et al. 2018). The monthly aerosol, water vapor, and cloud products from MODIS were produced from aggregating the respective daily products, with the same mapping grids and resolutions. On the other hand, the L3 daily products were produced from aggregating the respective L2 products in 1° × 1° spatial resolution. The initial horizontal resolution of L2 aerosol optical depth was 10km, of L2 water vapor, cloud optical depth, and cloud effective radius for both liquid and ice clouds 1km, and for L2 cloud fraction 5km. More details about the calculation and derivation of the MODIS products can be found in Hubanks et al. (2019) and Platnick et al. (2015).

In this work, we utilized the monthly mean aerosol optical depth at 550 nm (AOD) from the most recent DTB aerosol dataset (collection 6.1, 1° × 1° spatial resolution), over East Asia (EA) (20°–45° N, 105°–122.5°E) (Fig. 1), for the period July 2003–December 2018. AOD from MODIS instrument is found to be in good agreement and well-validated with AOD from ground-based measurements (Li et al. 2007; Xie et al. 2011; Luo et al. 2014; Wei et al. 2019). To investigate the aerosol–water vapor–cloud relations, we also used quasi-

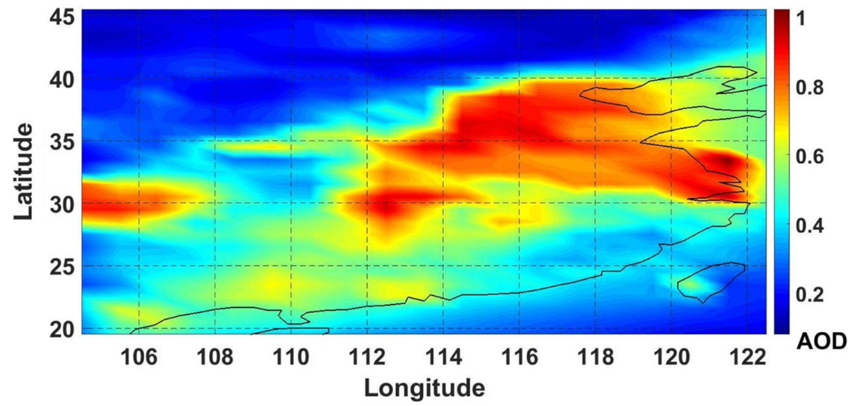

Fig. 1 The region of East Asia (EA) used in this study, with the monthly mean aerosol optical depth at 550 nm (AOD) from MODIS Aqua, for the period 2003–2018

coincident monthly mean data of cloud cover (CC), water vapor at clear sky (WV), cloud optical depth (COD), cloud effective radius-ice (CERI), and cloud effective radius-liquid (CERL) over the same region (Table 1). According to Gryspeerdt et al. (2014), quasi-coincident (provided in the same grid cell) aerosol–cloud data ensure that data are close enough to each other and represent the total time-integrated effect of aerosols on clouds.

Monthly products provide us with continuous time series that is essential for performing CCM method, instead of using daily products that may have missing values. In addition, monthly products have been widely used in many aerosol–cloud interactions studies utilizing long-term observations, since they are less noisy than daily products, minimizing the effect of local meteorology (Remer et al. 2005; Zhao et al. 2018b; Rao and Dey 2020). On the other hand, monthly products have the uncertainty of their partial daily values and the one cause of the aggregation procedure.

The above water vapor and cloud products from MODIS have been successfully compared and/or used in conjunction with other remote sensing data and model results and used in numerous previous studies investigating the aerosol–cloud interactions (Kumar 2013; Liu et al. 2017; Kant et al. 2019; Rao and Dey 2020).

2.2 Convergent cross mapping algorithm

Sugihara et al. (2012) developed the convergent cross mapping (CCM) method to identify causality especially in nonlinear dynamic systems with weak to moderate coupling. This method is based on Takens's (1981) theorem, which states that the essential information of a multidimensional dynamical system is retained in the time series of any single variable of that system. For example, if variables X and Y belong to the same dynamical system, each variable can reconstruct the attractor of the underlying dynamical system. CCM is related to simplex projection, which predicts a point in a time series X at a time $t+1$ (X_{t+1}), by using the values with the most similar histories to X_t (Sugihara and May 1990; Sugihara et al. 1990). In the same way, CCM uses the values with the most similar histories to X_t to estimate Y_t. In other words, it correlates the original time series of Y and an estimate of Y, made using its convergent cross mapping with X (McCracken and Weigel 2014). The CCM method consists of five steps. First, given an embedding dimension E, the shadow manifold of X (M_X) is created by associating a delay vector $\underline{\mathbf{x}}(\mathbf{t})$ to each point X_t in X for $1+(E\text{-}1)\tau < t < L$, where L is the library length (number of points in the time series) and τ is the time delay. Note that E is dependent on the properties of the data. Then, the $E+1$ nearest neighbors are searched for

Table 1 MODIS/Aqua parameters used in this study

Aerosol/cloud parameters	MODIS data variable
Aerosol optical depth at 550 nm (AOD)	AOD_550_Dark_Target_Deep_Blue_Combined_Mean_Mean
Cloud cover (CC)	Cloud_Fraction_Mean_Mean
Water vapor (WV)	Atmospheric_Water_Vapor_QA_Mean_Mean
Cloud optical depth (COD)	Cloud_Optical_Thickness_Combined_Mean_Mean
Cloud effective radius-ice (CERI)	Cloud_Effective_Radius_Ice_Mean_Mean
Cloud effective radius-liquid (CERL)	Cloud_Effective_Radius_Liquid_Mean_Mean

each M_{Xt}, where E+1 is the minimum number of points needed for a bounding simplex in an E-dimensional space, according to

$$d_{\mathrm{i}} = D[\underline{\mathbf{x}}(t), \underline{\mathbf{x}}(t_I)] \quad (1)$$

where $D[\underline{\mathbf{x}}(t), \underline{\mathbf{x}}(t_I)]$ is the Euclidean distance between vectors $\underline{\mathbf{x}}(t)$ and $\underline{\mathbf{x}}(t_I)$. Each of the E+1 nearest neighbors is used to compute the associated weight w_i, based on the distance between $\underline{\mathbf{x}}(t)$ and its ith nearest neighbor on $\boldsymbol{M_X}$ according to

$$w_i = u_i / \Sigma\, u_j \quad , \quad j = 1 \ldots E+1 \quad (2)$$

where

$$u_i = \exp\{-d[\underline{\mathbf{x}}(t), \underline{\mathbf{x}}(t_{\mathrm{i}})]/d[\underline{\mathbf{x}}(t), \underline{\mathbf{x}}(t_1)]\} \quad (3)$$

Y_t is then estimated in Y, from a locally weighted mean of the E+1 $Y(t_i)$ values, according to

$$\widehat{Y}(t) \mid \boldsymbol{M_X} = \Sigma\, w_i\, Y(t_{\mathrm{i}}) \quad i = 1 \ldots E+1 \quad (4)$$

Finally, the CCM correlation between Y_t and $\hat{Y}(t)|\boldsymbol{M_X}$, expressed with Pearson's correlation coefficient (ρ), is calculated (Fig. S2, Supplementary Material).

Note that a key property of CCM is convergence; that is, cross-mapped estimates improve in estimation skill with time series length L (sample size used to construct a library) (Packard et al. 1980; Sugihara and May 1990; Ascioti et al. 1993; Deyle and Sugihara 2011; Tsonis et al. 2015). For example, CCM tests for causation by measuring the extent to which the historical record of the affected variable Y reliably estimates states of a causal variable X, which is quantified by calculating the correlation coefficient ρ between predicted and observed X. If the estimation skill ρ increases with the length of the time series, it can be inferred that there is a direct or indirect causal effect of X on Y. We call this Y cross-maps X. For more details, see Supplementary Material.

CCM has been used successfully to identify causality in many cases where a weak to moderate forcing is the case (Sugihara et al. 2012 and references therein). In such cases, other approaches to infer causality such as Granger causality (Granger 1969) fail to establish directional influences. More details about CCM method can be found in Sugihara et al. (2012) and its respective Supplementary Materials.

In this work, the rEDM (Version 0.7.5) R package was used for applying the CCM method (https://cran.r-project.org/web/packages/rEDM/index.html), which is ideal for reconstructing the behavior of dynamic systems using time series data.

2.3 Methods and procedures

Since CCM is based on Takens's theorem, it requires that the time series we use are part of a nonlinear dynamical system. Thus, before we proceed with CCM, we first test the signals for nonlinearity. To determine whether a time series reflects linear or nonlinear processes, we compared the out-of-sample forecast skill of a linear model (AR) versus an equivalent nonlinear model. To do this, we applied a two-step procedure. Firstly, we used simplex projection (Sugihara and May 1990) to identify the best embedding dimension (E), based on prediction skill. Simplex projection is a nearest-neighbor forecasting algorithm that involves tracking the forward trajectory of nearby points in a lag coordinate embedding. The selection of the best E was made by using an exploratory series of 20 different embedding dimensions to evaluate the prediction. Secondly, we used this embedding in the S-map procedure (Sugihara 1994) to assess the nonlinearity of the time series, calculating the nonlinear tuning parameter θ, which defines the strength of the weighting when fitting the local linear map (see Supplementary Material for details). Then, we applied the CCM method to investigate the causality between AOD, WV, CC, COD, CERI, and CERL.

To examine the statistical significance of the CCM results, we generated randomized surrogate data (1000 values for each time series), following Ebisuzaki (1997), and we cross-mapped each time series with the surrogate one, generating a null distribution for ρ, against which the actual cross map ρ can be compared (e.g., AOD cross-maps surrogate CC, CC cross-maps surrogate AOD). In this way, we were able to calculate a p value for rejecting the null hypothesis that cross-mapped skill is driven by common seasonality.

Finally, to investigate if the causality between the parameters was truly bidirectional or just synchronous interactions, we calculated the cross-mapped skill of the time delay prediction parameter of CCM method (t_{p}), which denotes the time delay by which Y information is encoded in the time series of X. t_{p} values less than zero ($t_{\mathrm{p}} < 0$) correspond to estimating the past values of X, using the reconstructed states of Y (i.e., Y causes X), while tp values greater than zero ($t_{\mathrm{p}} > 0$) correspond to the fact that there is no causality in the reverse direction (i.e., Y does not cause X). t_{p} values equal to zero ($t_{\mathrm{p}} = 0$) states synchronous interactions between the variables. The methodology used in our work can be summarized in Fig. 2.

3 Results and discussion

To study the causality between aerosols, water vapor, and cloud parameters, we utilized monthly mean AOD, CC, WV, COD, CERI, and CERL data from MODIS/Aqua, over

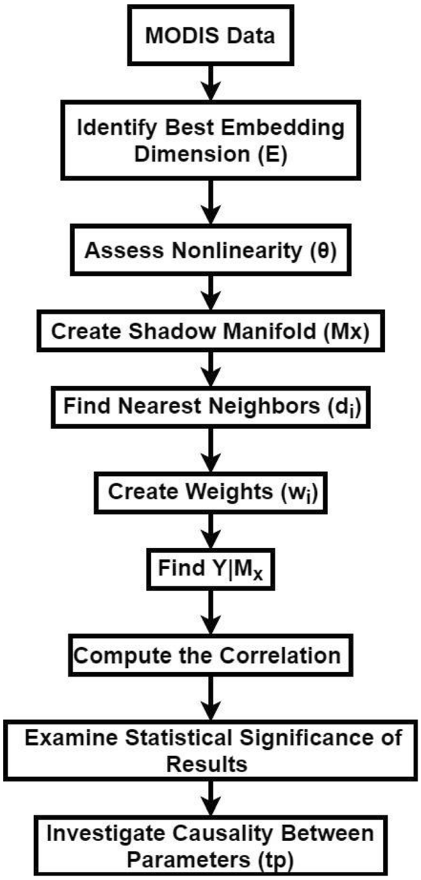

Fig. 2 Flowchart illustrating the methodology followed in this study

EA region, from July 2003–December 2018. The time series of the data are illustrated in Fig. S1 (Supplementary Material). To gain a first insight into the correlation of the variables, we applied a simple regression statistical analysis to the data (Fig. 3). A weak correlation was observed between AOD and CC (Pearson's correlation coefficient, $\rho = 0.2$), AOD and WV ($\rho = 0.094$), AOD and CERI ($\rho = -0.015$), and AOD and CERL ($\rho = -0.124$). A stronger correlation was observed between AOD and COD ($\rho = -0.413$), which is statistically significant at the 95% confidence level. Note that weak correlations do not necessarily imply no causality especially when we are dealing with nonlinear systems. For validation reasons, we also performed a Spearman statistical analysis, which is used in nonlinear systems, calculating Spearman's correlation coefficient (ρ_s) for the same pairs of variables. The results were similar to the ones that were found previously, using the regression analysis (Table S1, Supplementary Material).

To identify the best embedding dimension (E), we performed the simplex projection method (Sugihara and May 1990). The results of the simplex projection for AOD are shown in Fig. 4. The E with the maximum forecast skill (expressed with Pearson's correlation coefficient, ρ) was found to be 16 ($E = 16$, $\rho = 0.821$), based on 170 predictions. However, significant correlations were present for lower embeddings, as well, which is more desirable, especially for small data sizes, to preserve the sample size and avoid overfitting the model (Clark et al. 2015). For this reason, we chose $E = 7$ ($\rho = 0.702$), which was based on 179 predictions. We also conducted the same analysis for the other parameters

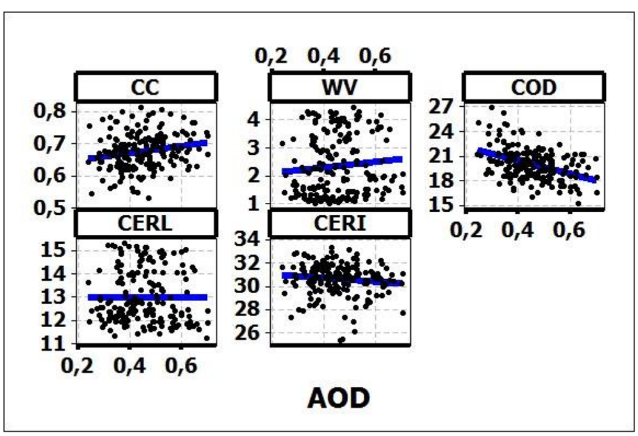

Fig. 3 Scatterplot of monthly mean aerosol optical depth at 550 nm (AOD), cloud cover (CC), water vapor in cm (WV), cloud optical depth (COD), cloud effective radius-ice in μm (CERI), and cloud effective radius-liquid in μm (CERL) from MODIS/Aqua, over East Asia (EA), for the period 2003–2018. The blue line represents the linear fit of the data

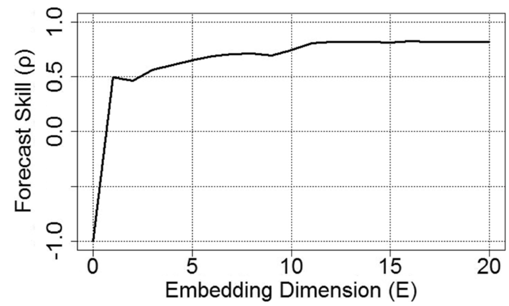

Fig. 4 Forecast skill expressed with Pearson's correlation coefficient (ρ) of the embedding dimension (E) for aerosol optical depth at 550 nm (AOD) time series

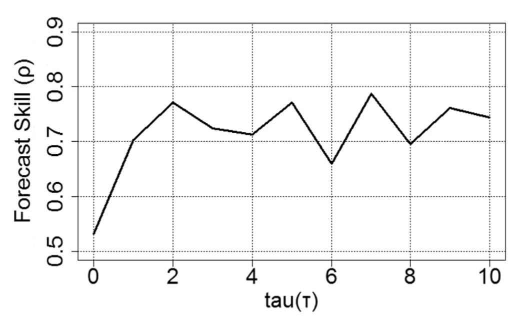

Fig. 5 Forecast skill expressed with Pearson's correlation coefficient (ρ) of the time delay embedding lag parameter (tau, τ) for embedding dimension (E) equals to 7, for aerosol optical depth at 550 nm (AOD) time series

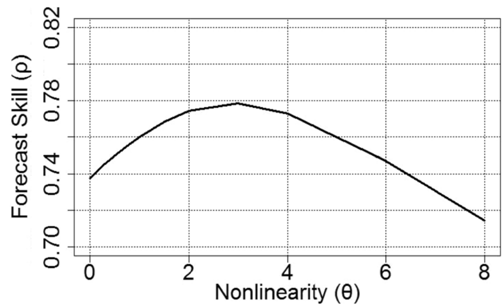

Fig. 6 Forecast skill expressed with Pearson's correlation coefficient (ρ) of the nonlinearity parameter (θ) for embedding dimension (E) equals to 7 and for time delay embedding lag parameter (τ) equals to 2, for aerosol optical depth at 550 nm (AOD) time series

(CC, WV, COD, CERI, CERL) and found that the optimum embedding dimension was equal to 7 (Fig. S3, Supplementary Material). The next step was to calculate the optimum time delay embedding lag (tau, τ) for $E = 7$, using the same method as before (simplex projection). The best τ value for $E = 7$ was found to be $\tau = 2$ ($\rho = 0.771$) for AOD (Fig. 5), as well as for the other parameters (Fig. S4, Supplementary Material).

The results for the S-map analysis for AOD and for the rest of the parameters are shown in Figs. 6 and S5 (Supplementary Material), respectively. This analysis is a simple test for nonlinear dynamics based on the relative ability to predict based on a linear stochastic (AR model) versus an analogous nonlinear model (Sugihara 1994). Evidence for nonlinear dynamics is demonstrated if forecast performance improves as the S-map model is tuned toward nonlinear solutions ($\theta > 0$) (Supplementary Material). As shown in Figs. 6 and S5 (Supplementary Material), this is indeed the case here. Thus, we can conclude that our system is nonlinear.

Finally, to test causality between AOD, CC, WV, COD, CERI, and CERL, we applied the CCM method for AOD with WV and with each cloud parameter separately (CC, COD, CERI, CERL), using the full time series as library, for $E = 7$ and $\tau = 2$ (Table S2, Supplementary Material). In addition, for comparison purposes and to investigate if seasonality affects the correlation between the parameters, we computed the lagged cross-correlation between the time series, allowing lags for up to ± 3 months (Table S3, Supplementary Material).

It was found that the cross-mapped results between the variables are higher than the correlation results, indicating that there is a causal effect between them. An exception was observed between AOD and COD, where the correlation (maximum absolute Pearson's correlation coefficient, $|\rho_{max}| = 0.413$) is higher than the cross-mapped skill ($\rho = 0.373$ for AOD cross mapping COD and $\rho = 0.360$ for COD cross mapping AOD). This could be a sign that AOD and COD share a common seasonality which hinders disentangling their cause-and-effect relation using CCM method. On the other hand, we cannot rule out that this might be a retrieval artifact of the MODIS sensor (Alam et al. 2014).

To quantify the convergence between the time series, we calculated the cross-mapped skill, using 80 different random libraries (L) for each variable, where each of them was comprised from 300 random subsamples of the time series. Figure 7 illustrates the mean cross-mapped skill expressed with Pearson's correlation coefficient (ρ) for each library size, among the time series, for $E = 7$ and $\tau = 2$. Note that CCM method cannot present the positive or the negative effect between the driving and the response variables clearly. It only states if there is a connection among them and the direction of the forcing.

It was found that AOD cross-maps CC (CC has an effect on AOD), as well as CC cross-maps AOD (AOD has an effect on CC), since ρ increases as L is increasing (Fig. 7a). The effect of aerosols on CC has been observed in many previous studies (Kourtidis et al. 2015; Stathopoulos et al. 2017; Kudzotsa et al. 2019). In particular, aerosols can serve as cloud condensation nuclei (CCN), causing an increase in the number of cloud droplets, affecting cloud formation and cloud cover. On the other hand, the effect of CC on AOD can be attributed to the misclassification of AOD as CC from MODIS instrument (Ten Hoeve et al. 2011). It seems to exist a bidirectional cause-and-effect relation between AOD and WV (Fig. 7b). When aerosols are found inside a water vapor laden environment, a fraction of them becomes activated as CCN, growing in size, which may increase the AOD (Feingold et al. 2003). When more aerosol particles are inserted in this environment, the already activated large particles suppress supersaturation at the early stages of activation, altering the available amount of water vapor for further condensational growth (Feingold et al. 2001). In addition, a bidirectional causality was found between AOD and COD (Fig. 7c). An increase of aerosol concentration can result in an increase of COD, through the invigoration effect of aerosols on clouds mechanism (Koren et al. 2014). On the other hand, dark aerosols above the clouds can reduce the reflectance observed by MODIS sensor, leading to a retrieval artifact (Alam et al. 2014). This may explain the convergence between COD and AOD (AOD cross-maps COD). CERI was found to influence AOD (AOD cross-maps CERI), as well as AOD was found to affect CERI (CERI cross-maps AOD) (Fig. 7d). According to Stevens and Feingold (2009), as AOD increases (higher aerosol loading), more smaller droplets are produced that delay the ability of clouds to precipitate. This delay allows the droplets to be transported higher in the atmosphere, where a fraction of them transforms into ice particles. This amount of ice nuclei can possibly increase the growth of ice crystals which, in turn, can increase the scattering of shortwave radiation (Kant et al. 2019). Finally, we found a bidirectional cause-and-

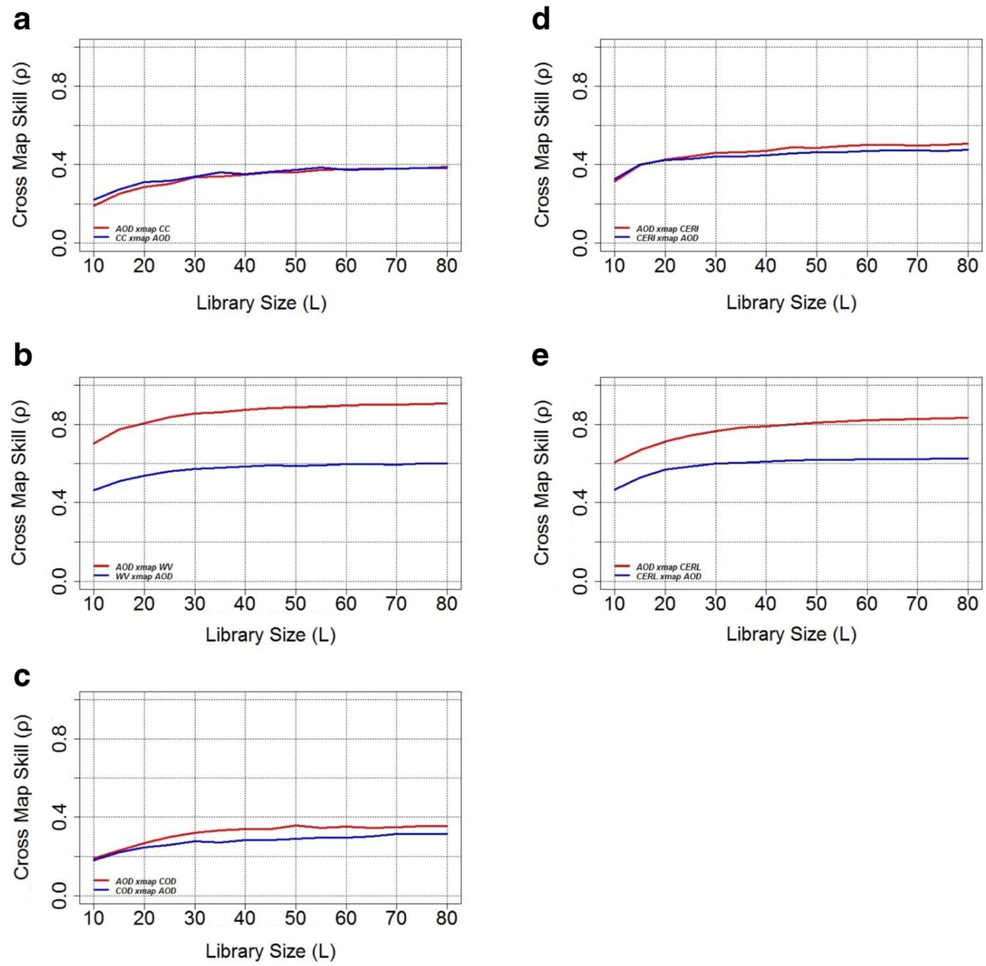

Fig. 7 Cross-mapped skill expressed with Pearson's correlation coefficient (ρ) as a function of library size (L) **a** for aerosol optical depth at 550 nm (AOD)–cloud cover (CC), **b** for AOD–water vapor (WV), **c** for AOD–cloud optical depth (COD), **d** for AOD–cloud effective radius-ice (CERI), and **e** for AOD–cloud effective radius-liquid (CERL), for embedding dimension (E) equals to 7 and for time delay embedding lag parameter (τ) equals to 2. xmap denotes cross mapping which is translated as Y parameter affects X parameter

effect relation between AOD and CERL (Fig. 7e). This may be a sign of first indirect effect of aerosols on clouds (Twomey 1974), since aerosols, acting as CCN, can increase cloud droplet number, with a simultaneous decrease in cloud effective radius (CER). To validate our results, we conducted sensitivity tests for the same time series for $E = 6$ and $E = 8$ (Figs. S6, S7, Supplementary Material). Note that the behavior of the variables is identical as in Fig. 7.

To examine the statistical significance of the results, we generated randomized surrogate data (1000 values for each time series), following Ebisuzaki (1997), and we cross-mapped each time series with the surrogate one. Our investigation showed that not only the cross-mapped skills calculated for the real time series are better than the median expectation, under the null hypothesis, but also they are statistically significant at 95% confidence level ($p < 0.05$). In addition, this is an indication that eventually, AOD and COD do not share a common seasonality and that there is indeed causality between the two parameters, even though the $|\rho_{max}|$ was previously found to be higher than the cross-mapped skill.

Since atmosphere is a dynamic system, the remaining question is how many of the above cause-and-effect relations are truly bidirectional or just synchronous interactions. To investigate this aspect, we calculated the cross-mapped skill of the time delay prediction parameter of CCM method (t_p) (Fig. 8). For validation purposes, we performed sensitivity tests with the same method, for $E = 6$ (Fig. S8, Supplementary Material) and $E = 8$ (Fig. S9, Supplementary Material). The maximum ρ (ρ_{max}) for each pair of parameters and for the different embedding dimensions ($E = 6$–8) is listed in Table 2.

From the sensitivity analysis, it is obvious that there is a bidirectional forcing among AOD–CC, AOD–WV, AOD–COD, and AOD–CERL, since the corresponding t_p values were less or equal to zero (Fig. 8, Table 2). Note that, for certain E, the closer the negative t_p values is to zero, the faster the causal interaction is between the parameters. For

Table 2 Maximum Pearson's correlation coefficient (ρ_{max}) and the corresponding time delay prediction parameter (t_p) value for the AOD–CC–WV–COD–CERI–CERL cross mapping relations for embedding dimensions 6–8 (E=6–8). xmap denotes cross mapping which is translated as Y parameter affects X parameter

	E=6		E=7		E=8	
	Time prediction (t_p)	Maximum Pearson's correlation coefficient (ρ_{max})	Time prediction (t_p)	Maximum Pearson's correlation coefficient (ρ_{max})	Time prediction (t_p)	Maximum Pearson's correlation coefficient (ρ_{max})
AOD xmap CC	−10	0.381	−10	0.386	−2	0.398
CC xmap AOD	−2	0.375	+2	0.404	0	0.423
AOD xmap WV	−9	0.876	−4	0.893	−5	0.888
WV xmap AOD	−10	0.610	−10	0.612	−10	0.613
AOD xmap COD	−10	0.315	+4	0.322	−10	0.324
COD xmap AOD	−9	0.262	0	0.274	0	0.278
AOD xmap CERI	+8	0.508	+10	0.518	+8	0.520
CERI xmap AOD	+2	0.454	+2	0.480	+2	0.485
AOD xmap CERL	−10	0.806	−8	0.826	+5	0.827
CERL xmap AOD	−9	0.613	−9	0.616	−9	0.622

example, the effect of WV on AOD (AOD cross-maps WV, t_p = −4 for E = 7) and the effect of CERL on AOD (AOD cross-maps CERL, t_p = −8 for E = 7) are found to be faster than the effect of AOD on WV (WV cross-maps AOD, t_p = −10 for E = 7) and the effect of AOD on CERL (CERL cross-maps AOD, t_p = −9 for E = 7), respectively (Fig. 8b, e, Table 2). Nonetheless, in some cases, t_p was found to be greater than zero (CC cross-maps AOD for E = 7, AOD cross-maps COD for E = 7, and AOD cross-maps CERL for E = 8), but the total forcing from the sensitivity analyses (2/3 of the results) indicate a bidirectional cause-and-effect relation, with the effect of AOD on CC to be faster than the effect of CC on AOD, the effect of AOD on COD to be faster than the effect of COD on AOD and the effect of CERL on AOD to be faster than the effect of AOD on CERL (as mentioned before). Surprisingly, t_p for AOD–CERI was found to be greater than zero, even though it seemed to exist a convergence between them (Figs. 7d and 8d). Hence, there is no causality between the two time series, probably because of strong coupling between aerosols and ice nuclei (Wang et al. 2019). In general, when strong coupling exists between two variables (X, Y), then the Y variable is completely controlled by X and the feature of Y variable is exactly similar to X variable, which may lead to erroneous bidirectional detection (Rulkov et al. 1995; Josic 2000).

4 Conclusions

In this work, we investigated the cause-and-effect relations between aerosols, water vapor, and clouds over East Asia (20°–45° N, 105°–122.5° E), utilizing remote sensing data from the Moderate Resolution Imaging Spectro-radiometer (MODIS) sensor onboard Aqua satellite. In particular, we used monthly mean data of aerosol optical depth at 550 nm (AOD) with quasi-coincident monthly mean data of water vapor at clear sky (WV), cloud cover (CC), cloud optical depth (COD), cloud effective radius-ice (CERI), and cloud effective radius-liquid (CERL), for the period July 2003–December 2018, using convergent cross mapping (CCM) method. To detect the causality between the time series, we calculated the cross-mapped skill for each pair of variables, expressed with Pearson's correlation coefficient (ρ). In addition, we examined the direction of the forcing using the time delay prediction parameter of CCM.

AOD–CC and AOD–COD variables were found to have a bidirectional forcing, with the effect of AOD on CC and COD to be faster than the effect of CC and COD on AOD, which could be attributed to the invigoration effect of aerosols on clouds (AOD affects CC and COD) and probably to retrieval artifact from MODIS sensor (CC and COD affect AOD). AOD–WV variables were also found to have a bidirectional cause-and-effect relation, with the effect of WV on AOD to be

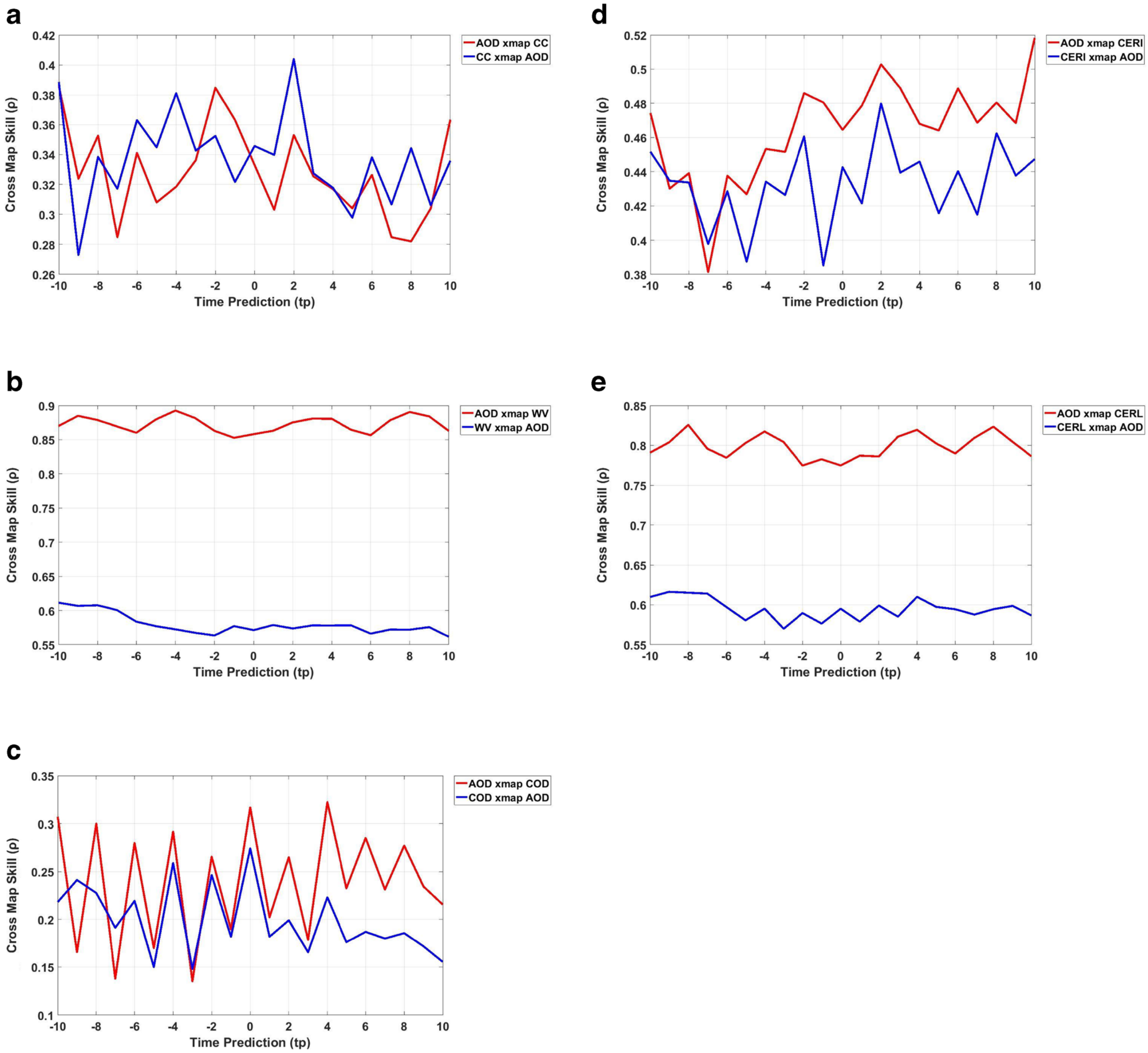

Fig. 8 Cross-mapped skill expressed with Pearson's correlation coefficient (ρ) as a function of convergent cross mapping's (CCM) time delay prediction parameter (t_p) **a** for aerosol optical depth at 550 nm (AOD)–cloud cover (CC), **b** for AOD–water vapor (WV), **c** for AOD–cloud optical depth (COD), **d** for AOD–cloud effective radius-ice (CERI), and **e** for AOD–cloud effective radius-liquid (CERL), for embedding dimension (E) equals to 7 and for time delay embedding lag parameter (τ) equals to 2. xmap denotes cross mapping which is translated as Y parameter affects X parameter. Note that each sub-figure has different y-axis for clarity

faster than the effect of AOD on WV. This relation can be ascribed to the fact that WV can activate aerosols to condensate, transforming to cloud condensation nuclei (CCN) (WV affects AOD), while these large CCN can alter the available amount of water vapor for further condensational growth (AOD affects WV). Furthermore, AOD–CERL time series present a bidirectional forcing, as well (with the effect of CERL on AOD to be faster than the effect of AOD on CERL), which could be attributed to the first indirect effect of aerosols on clouds. Finally, we didn't find causality between AOD and CERI, probably because of strong coupling among aerosols and ice nuclei. The above inter-relations are illustrated in Fig. 9.

To conclude, and based on the above findings, CCM method can effectively be used in all aerosol–cloud interactions' studies, searching for causality among the parameters.

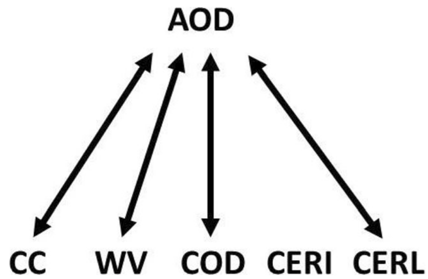

Fig. 9 Schematic illustration of inter-relations between aerosol optical depth at 550 nm (AOD), cloud cover (CC), water vapor (WV), cloud optical depth (COD), cloud effective radius-ice (CERI), and cloud effective radius-liquid (CERL) over East Asian region

Supplementary Information The online version contains supplementary material available at https://doi.org/10.1007/s00704-021-03563-7.

Acknowledgements The authors would like to thank NASA's Earth Observing System Data and Information System (EOSDIS), for providing MODIS Aqua aerosol, water vapor, and cloud data used in this study, through GIOVANNI website (https://giovanni.gsfc.nasa.gov/giovanni/) and the rEDM developing team for the provision of rEDM R package (https://ha0ye.github.io/rEDM/index.html). The authors would also like to thank the anonymous reviewers for their detailed comments and suggestions that substantially improved the quality of this manuscript.

Author contribution All authors contributed to the study conception and design. Material preparation, data collection, and analysis were performed by Stavros Stathopoulos, Anastasios A. Tsonis, and Konstantinos Kourtidis. The first draft of the manuscript was written by Stavros Stathopoulos and all authors commented on previous versions of the manuscript. All authors read and approved the final manuscript.

Data and materials availability Available after request

Code availability Available after request

Declarations

Competing interests The authors declare no competing interests.
Supplementary Information The online version contains supplementary material available at https://doi.org/10.1007/s00704-021-03563-7.

References

Ackerman AS, Toon OB, Stevens DE et al (2000) Reduction of tropical cloudiness by soot. Science (80-) 288:1042–1047. https://doi.org/10.1126/science.288.5468.1042

Alam K, Khan R, Blaschke T, Mukhtiar A (2014) Variability of aerosol optical depth and their impact on cloud properties in Pakistan. J Atmos Solar-Terrestrial Phys 107:104–112. https://doi.org/10.1016/j.jastp.2013.11.012

Albrecht BA (1989) Aerosols, cloud microphysics, and fractional cloudiness. Science 245:1227–1230. https://doi.org/10.1126/science.245.4923.1227

Andreae MO, Rosenfeld D (2008) Aerosol–cloud–precipitation interactions. Part 1. The nature and sources of cloud-active aerosols. Earth-Science Rev 89:13–41. https://doi.org/10.1016/j.earscirev.2008.03.001

Ascioti FA, Beltrami E, Carroll TO, Wirick C (1993) Is there chaos in plankton dynamics? J Plankton Res 15:603–617. https://doi.org/10.1093/plankt/15.6.603

Clark AT, Ye H, Isbell F, Deyle ER, Cowles J, Tilman GD, Sugihara G (2015) Spatial convergent cross mapping to detect causal relationships from short time series. Ecology 96:1174–1181. https://doi.org/10.1890/14-1479.1

Deyle ER, Sugihara G (2011) Generalized theorems for nonlinear state space reconstruction. PLoS One 6:e18295. https://doi.org/10.1371/journal.pone.0018295

Ebisuzaki W (1997) A method to estimate the statistical significance of a correlation when the data are serially correlated. J Clim 10:2147–2153. https://doi.org/10.1175/1520-0442(1997)010<2147:AMTETS>2.0.CO;2

Eck TF, Holben BN, Reid JS, Xian P, Giles DM, Sinyuk A, Smirnov A, Schafer JS, Slutsker I, Kim J, Koo JH, Choi M, Kim KC, Sano I, Arola A, Sayer AM, Levy RC, Munchak LA, O'Neill NT, Lyapustin A, Hsu NC, Randles CA, da Silva AM, Buchard V, Govindaraju RC, Hyer E, Crawford JH, Wang P, Xia X (2018) Observations of the interaction and transport of fine mode aerosols with cloud and/or fog in Northeast Asia from aerosol robotic network and satellite remote sensing. J Geophys Res Atmos 123:5560–5587. https://doi.org/10.1029/2018JD028313

Feingold G, Eberhard WL, Veron DE, Previdi M (2003) First measurements of the Twomey indirect effect using ground-based remote sensors. Geophys Res Lett 30:19–22. https://doi.org/10.1029/2002GL016633

Feingold G, Remer LA, Ramaprasad J, Kaufman YJ (2001) Analysis of smoke impact on clouds in Brazilian biomass burning regions: an extension of Twomey's approach. J Geophys Res 106:22907–22922. https://doi.org/10.1029/2001JD000732

Gao B-C, Kaufman YJ (1998) The MODIS near-IR water vapor algorithm. Available online at: https://atmosphere-imager.gsfc.nasa.gov/documentation/atbds-plans-guides. Accessed 22 December 2020

Grandey BS, Stier P, Wagner TM (2013) Investigating relationships between aerosol optical depth and cloud fraction using satellite, aerosol reanalysis and general circulation model data. Atmos Chem Phys 13:3177–3184. https://doi.org/10.5194/acp-13-3177-2013

Granger CWJ (1969) Investigating causal relations by econometric models and cross-spectral methods. Econometrica 37:424. https://doi.org/10.2307/1912791

Gryspeerdt E, Stier P, Partridge DG (2014) Satellite observations of cloud regime development: the role of aerosol processes. Atmos Chem Phys 14:1141–1158. https://doi.org/10.5194/acp-14-1141-2014

Hansen J, Sato M, Ruedy R (1997) Radiative forcing and climate response. J Geophys Res Atmos 102:6831–6864. https://doi.org/10.1029/96JD03436

Haywood J, Boucher O (2000) Estimates of the direct and indirect radiative forcing due to tropospheric aerosols: a review. Rev Geophys 38:513–543. https://doi.org/10.1029/1999RG000078

Heskamp L, Abeelen ASSM den, Lagro J, Claassen JAHR (2014) Convergent cross mapping: a promising technique for cerebral autoregulation estimation. Int J Clin Neurosci Ment Heal S20. https://doi.org/10.21035/ijcnmh.2014.1(Suppl.1).S20

Hodzic A, Duvel JP (2018) Impact of biomass burning aerosols on the diurnal cycle of convective clouds and precipitation over a tropical island. J Geophys Res Atmos 123:1017–1036. https://doi.org/10.1002/2017JD027521

Hsu NC, Jeong M-J, Bettenhausen C, Sayer AM, Hansell R, Seftor CS, Huang J, Tsay SC (2013) Enhanced deep blue aerosol retrieval algorithm: the second generation. J Geophys Res Atmos 118:9296–9315. https://doi.org/10.1002/jgrd.50712

Huang J, Lin B, Minnis P, Wang T, Wang X, Hu Y, Yi Y, Ayers JK (2006) Satellite-based assessment of possible dust aerosols semi-direct effect on cloud water path over East Asia. Geophys Res Lett 33:L19802. https://doi.org/10.1029/2006GL026561

Huang J, Minnis P, Chen B, Huang Z, Liu Z, Zhao Q, Yi Y, Ayers JK (2008) Long-range transport and vertical structure of Asian dust from CALIPSO and surface measurements during PACDEX. J Geophys Res 113:D23212. https://doi.org/10.1029/2008JD010620

Hubanks PA, King MD, Platnick S, Pincus R (2019) MODIS algorithm theoretical basis document no. ATBD-MOD-30 for Level-3 global gridded atmosphere products (08_D3, 08_E3, 08_M3) and users guide. Available online at https://atmosphere-imager.gsfc.nasa.gov/products/monthly) Accessed 22 December 2020

Jones TA, Christopher SA (2010) Statistical properties of aerosol-cloud-precipitation interactions in South America. Atmos Chem Phys 10: 2287–2305. https://doi.org/10.5194/acp-10-2287-2010, 2010

Josic K (2000) Synchronization of chaotic systems and invariant manifolds. Nonlinearity 13:1321–1336. https://doi.org/10.1088/0951-7715/13/4/318

Kant S, Panda J, Gautam R (2019) A seasonal analysis of aerosol-cloud-radiation interaction over Indian region during 2000–2017. Atmos Environ 201:212–222. https://doi.org/10.1016/j.atmosenv.2018.12.044

Koren I, Dagan G, Altaratz O (2014) From aerosol-limited to invigoration of warm convective clouds. Science (80-) 344:1143–1146. https://doi.org/10.1126/science.1252595

Koren I, Kaufman YJ, Rosenfeld D, Remer LA, Rudich Y (2005) Aerosol invigoration and restructuring of Atlantic convective clouds. Geophys Res Lett 32:n/a-n/a. https://doi.org/10.1029/2005GL023187

Kourtidis K, Stathopoulos S, Georgoulias AK, Alexandri G, Rapsomanikis S (2015) A study of the impact of synoptic weather conditions and water vapor on aerosol–cloud relationships over major urban clusters of China. Atmos Chem Phys 15:10955–10964. https://doi.org/10.5194/acp-15-10955-2015

Kudzotsa I, Dobbie S, Phillips V (2019) Modeled aerosol-cloud indirect effects and processes based on an observed partially glaciated marine deep convective cloud case. Atmos Environ 204:12–21. https://doi.org/10.1016/j.atmosenv.2019.02.010

Kumar A (2013) Variability of aerosol optical depth and cloud parameters over North Eastern regions of India retrieved from MODIS satellite data. J Atmos Solar-Terrestrial Phys 100–101:34–49. https://doi.org/10.1016/j.jastp.2013.03.025

Levy RC, Mattoo S, Munchak LA, Remer LA, Sayer AM, Patadia F, Hsu NC (2013) The Collection 6 MODIS aerosol products over land and ocean. Atmos Meas Tech 6:2989–3034. https://doi.org/10.5194/amt-6-2989-2013

Levy RC, Remer LA, Dubovik O (2007) Global aerosol optical properties and application to Moderate Resolution Imaging Spectroradiometer aerosol retrieval over land. J Geophys Res 112:D13210. https://doi.org/10.1029/2006JD007815

Li Z, Li C, Chen H, et al (2011) East Asian studies of tropospheric aerosols and their impact on regional climate (EAST-AIRC): an overview. J Geophys Res 116:D00K34. 10.1029/2010JD015257

Li Z, Niu F, Lee K-H, et al (2007) Validation and understanding of Moderate Resolution Imaging Spectroradiometer aerosol products (C5) using ground-based measurements from the handheld Sun photometer network in China. J Geophys Res 112:D22S09. https://doi.org/10.1029/2007JD008479

Liu J, Li Z (2018) Significant underestimation in the optically based estimation of the aerosol first indirect effect induced by the aerosol swelling effect. Geophys Res Lett 45:5690–5699. https://doi.org/10.1029/2018GL077679

Liu Y, de Leeuw G, Kerminen V-M, Zhang J, Zhou P, Nie W, Qi X, Hong J, Wang Y, Ding A, Guo H, Krüger O, Kulmala M, Petäjä T (2017) Analysis of aerosol effects on warm clouds over the Yangtze River Delta from multi-sensor satellite observations. Atmos Chem Phys 17:5623–5641. https://doi.org/10.5194/acp-17-5623-2017

Luo Y, Zheng X, Zhao T, Chen J (2014) A climatology of aerosol optical depth over China from recent 10 years of MODIS remote sensing data. Int J Climatol 34:863–870. https://doi.org/10.1002/joc.3728

McCracken JM, Weigel RS (2014) Convergent cross-mapping and pairwise asymmetric inference. Phys Rev E - Stat Nonlinear, Soft Matter Phys 90:1–7. https://doi.org/10.1103/PhysRevE.90.062903

Nakajima T, King MD (1990) Determination of the optical thickness and effective particle radius of clouds from reflected solar radiation measurements. Part I: theory. J Atmos Sci 47:1878–1893. https://doi.org/10.1175/1520-0469(1990)047<1878:DOTOTA>2.0.CO;2

Packard NH, Crutchfield JP, Farmer JD, Shaw RS (1980) Geometry from a time series. Phys Rev Lett 45:712–716. https://doi.org/10.1103/PhysRevLett.45.712

Park S-Y, Lee H-J, Kang J-E, Lee T, Kim C-H (2018) Aerosol radiative effects on mesoscale cloud–precipitation variables over Northeast Asia during the MAPS-Seoul 2015 campaign. Atmos Environ 172:109–123. https://doi.org/10.1016/j.atmosenv.2017.10.044

Platnick S, King M, Hubanks P (2015) MODIS atmosphere L3 monthly product. NASA MODIS Adaptive Processing System. Goddard Space Flight Center, USA. Available online at: https://doi.org/10.5067/MODIS/MOD08_M3.006. Accessed 22 December 2020

Platnick S, King MD, Mayer K, Wind G, Amarasinghe N, Marchant B, Arnold G, Zhang Z, Hubanks P, Ridgway B, Riedi J, (2018) ' MODIS cloud optical properties: user guide for the collection 6/6.1 Level-2 MOD06/MYD06 product and associated Level-3 datasets version 1.1. Available online at: https://atmosphere-imager.gsfc.nasa.gov/documentation/atbds-plans-guides. Accessed 22 December 2020

Rao S, Dey S (2020) Consistent signal of aerosol indirect and semi-direct effect on water clouds in the oceanic regions adjacent to the Indian subcontinent. Atmos Res 232:104677. https://doi.org/10.1016/j.atmosres.2019.104677

Remer LA, Kaufman YJ, Tanré D, Mattoo S, Chu DA, Martins JV, Li RR, Ichoku C, Levy RC, Kleidman RG, Eck TF, Vermote E, Holben BN (2005) The MODIS aerosol algorithm, products, and validation. J Atmos Sci 62:947–973. https://doi.org/10.1175/JAS3385.1

Rulkov NF, Sushchik MM, Tsimring LS, Abarbanel HDI (1995) Generalized synchronization of chaos in directionally coupled chaotic systems. Phys Rev E 51:980–994. https://doi.org/10.1103/PhysRevE.51.980

Shi YR, Levy RC, Eck TF, Fisher B, Mattoo S, Remer LA, Slutsker I, Zhang J (2019) Characterizing the 2015 Indonesia fire event using modified MODIS aerosol retrievals. Atmos Chem Phys 19:259–274. https://doi.org/10.5194/acp-19-259-2019

Solomos S, Bougiatioti A, Soupiona O, Papayannis A, Mylonaki M, Papanikolaou C, Argyrouli A, Nenes A (2019) Effects of regional and local atmospheric dynamics on the aerosol and CCN load over Athens. Atmos Environ 197:53–65. https://doi.org/10.1016/j.atmosenv.2018.10.025

Stathopoulos S, Georgoulias AK, Kourtidis K (2017) Space-borne observations of aerosol - cloud relations for cloud systems of different heights. Atmos Res 183:191–201. https://doi.org/10.1016/j.atmosres.2016.09.005

Stevens B, Feingold G (2009) Untangling aerosol effects on clouds and precipitation in a buffered system. Nature 461:607–613. https://doi.org/10.1038/nature08281

Sugihara G (1994) Nonlinear forecasting for the classification of natural time series. Philos Trans R Soc London Ser A Phys Eng Sci 348: 477–495. https://doi.org/10.1098/rsta.1994.0106

Sugihara G, Grenfell B, May RM (1990) Distinguishing error from chaos in ecological time series. Philos Trans - R Soc London, B 330:235–251. https://doi.org/10.1098/rstb.1990.0195

Sugihara G, May R, Ye H et al (2012) Detecting causality in complex ecosystems. Science (80-) 338:496–500. https://doi.org/10.1126/science.1227079

Sugihara G, May RM (1990) Nonlinear forecasting as a way of distinguishing chaos from measurement error in time series. Nature 344:734–741. https://doi.org/10.1038/344734a0

Takens F (1981) Detecting strange attractors in turbulence. In: Rand D, Young LS (eds) Dynamical Systems and Turbulence, Warwick 1980, Lecture Notes in Mathematics, vol 898. Springer, Berlin, Heidelberg

Team M C M, Ackerman S, Strabala K, Menzel P, Frey R, et al (2010) Discriminating clear-sky from cloud with modis algorithm theoretical basis document (mod35). Cooperative Institute for Meteorological Satellite Studies, University of Wisconsin – Madison. Available online at: https://atmosphere-imager.gsfc.nasa.gov/documentation/atbds-plans-guides. Accessed 22 December 2020

Ten Hoeve JE, Remer LA, Jacobson MZ (2011) Microphysical and radiative effects of aerosols on warm clouds during the Amazon biomass burning season as observed by MODIS: impacts of water vapor and land cover. Atmos Chem Phys 11:3021–3036. https://doi.org/10.5194/acp-11-3021-2011

Tsonis AA, Deyle ER, May RM, Sugihara G, Swanson K, Verbeten JD, Wang G (2015) Dynamical evidence for causality between galactic cosmic rays and interannual variation in global temperature. Proc Natl Acad Sci 112:3253–3256. https://doi.org/10.1073/pnas.1420291112

Twomey S (1974) Pollution and the planetary albedo. Atmos Environ 8:1251–1256. https://doi.org/10.1016/0004-6981(74)90004-3

Wang F, Guo J, Wu Y, Zhang X, Deng M, Li X, Zhang J, Zhao J (2014a) Satellite observed aerosol-induced variability in warm cloud properties under different meteorological conditions over eastern China. Atmos Environ 84:122–132. https://doi.org/10.1016/j.atmosenv.2013.11.018

Wang SX, Zhao B, Cai SY, Klimont Z, Nielsen CP, Morikawa T, Woo JH, Kim Y, Fu X, Xu JY, Hao JM, He KB (2014b) Emission trends and mitigation options for air pollutants in East Asia. Atmos Chem Phys 14:6571–6603. https://doi.org/10.5194/acp-14-6571-2014

Wang Y, Hu F, Cao Y, Yuan X, Yang C (2019) Improved CCM for variable causality detection in complex systems. Control Eng Pract 83:67–82. https://doi.org/10.1016/j.conengprac.2018.10.005

Wei J, Li Z, Peng Y, Sun L (2019) MODIS Collection 6.1 aerosol optical depth products over land and ocean: validation and comparison. Atmos Environ 201:428–440. https://doi.org/10.1016/j.atmosenv.2018.12.004

Xie Y, Zhang Y, Xiong X, Qu JJ, Che H (2011) Validation of MODIS aerosol optical depth product over China using CARSNET measurements. Atmos Environ 45:5970–5978. https://doi.org/10.1016/j.atmosenv.2011.08.002

Zhang D, Liu D, Luo T, Wang Z, Yin Y (2015) Aerosol impacts on cloud thermodynamic phase change over East Asia observed with CALIPSO and CloudSat measurements. J Geophys Res Atmos 120:1490–1501. https://doi.org/10.1002/2014JD022630

Zhang N, Wang G, Tsonis AA (2019) Dynamical evidence for causality between Northern Hemisphere annular mode and winter surface air temperature over Northeast Asia. Clim Dyn 52:3175–3182. https://doi.org/10.1007/s00382-018-4317-x

Zhao B, Gu Y, Liou K et al (2018a) Type-dependent responses of ice cloud properties to aerosols from satellite retrievals. Geophys Res Lett 45:3297–3306. https://doi.org/10.1002/2018GL077261

Zhao X, Liu Y, Yu F, Heidinger AK (2018b) Using long-term satellite observations to identify sensitive regimes and active regions of aerosol indirect effects for liquid clouds over global oceans. J Geophys Res Atmos 123:457–472. https://doi.org/10.1002/2017JD027187